

Control Color: Multimodal Diffusion-based Interactive Image Colorization

Zhexin Liang Zhaochen Li Shangchen Zhou Chongyi Li Chen Change Loy
S-Lab, Nanyang Technological University

{zliang008, c170086, s200094, ccloy}@ntu.edu.sg, lichongyi25@gmail.com

https://zhexinliang.github.io/Control_Color



Figure 1. The proposed CtrlColor achieves highly controllable image colorization, offering users a simple and intuitive means to colorize images according to their specific preferences. Our method supports both unconditional and conditional colorization, including options such as text, stroke, and exemplar image, as well as allows for any combination of them. Utilizing strokes as masks, our method facilitates selective image editing effortlessly. Our method also supports highly flexible iterative image editing, empowering users to finely tune specific details during the colorization process.

Abstract

Despite the existence of numerous colorization methods, several limitations still exist, such as lack of user interaction, inflexibility in local colorization, unnatural color rendering, insufficient color variation, and color overflow. To solve these issues, we introduce Control Color (CtrlColor), a multi-modal colorization method that leverages the pre-trained Stable Diffusion (SD) model, offering promising capabilities in highly controllable interactive image colorization. While several diffusion-based methods have been proposed, supporting colorization in multiple modalities remains non-trivial. In this study, we aim to tackle both unconditional and conditional image colorization (text

prompts, strokes, exemplars) and address color overflow and incorrect color within a unified framework. Specifically, we present an effective way to encode user strokes to enable precise local color manipulation and employ a practical way to constrain the color distribution similar to exemplars. Apart from accepting text prompts as conditions, these designs add versatility to our approach. We also introduce a novel module based on self-attention and a content-guided deformable autoencoder to address the long-standing issues of color overflow and inaccurate coloring. Extensive comparisons show that our model outperforms state-of-the-art image colorization methods both qualitatively and quantitatively.

1. Introduction

Image colorization aims at colorizing grayscale images, which enhances the visual appeal in various domains such as historical footage. Manual colorization is a labor-intensive process that heavily relies on the preferences, experience, imagination, and laborious effort of colorists.

Although many automatic colorization methods [7, 20, 25, 26, 37, 42, 44, 47–50, 54, 57] have been developed, they still exhibit certain drawbacks. These include limited color richness, color overflow, color distortions, and incomplete coloring in certain areas. Furthermore, methods that rely on user-provided conditions lack flexibility and precision. For example, these kinds of methods do not allow for selective colorization of specific regions or the use of strokes to apply color to particular objects. Recent image colorization techniques, such as those in UniColor [20] and iColoriT [50], offer stroke-based color control but are constrained to minor square hint points within object boundaries. This necessitates more exact hint placement, and the methods may struggle with significant color overflow when colorizing small areas or cannot correctly colorize images based on stroke’s color, as depicted in Fig. 2. In addition, these approaches do not facilitate region colorization due to their simplistic designs, which merely extend the hint point colors to adjacent regions.

Stable Diffusion (SD) [36] with ControlNet [53], which was originally proposed for conditional image generation, appears to be a viable solution for image colorization. Although it is capable of generating diverse and high-quality images with flexible conditions, it does not explore how to integrate multiple conditions within a unified framework, relying instead on a single control such as Canny edges or segmentation maps. Furthermore, due to the high sparsity of conditions and the inherent randomness in the diffusion process, it tends to generate results with low fidelity, making it unsuitable for our multimodal image colorization task.

To address the challenges mentioned above, we propose a novel multi-modal diffusion-based colorization framework, called CtrlColor. This framework aims to unify various colorization tasks including unconditional, prompt-, stroke-, and exemplar-based image colorization within a single framework. CtrlColor leverages rich priors encapsulated in the latent diffusion model (*i.e.*, SD [36]) that is trained on a large-scale image dataset. This enables our method to obtain significantly superior results compared to previous approaches in terms of color richness and diversity.

To address the color overflow and incorrect color issues, we introduce self-attention guidance and content-guided deformable autoencoder in our framework. Without any training, self-attention guidance is added in the inference process to address the small color overflow problem by blurring the out-of-distribution attention area and regenerating the blurred area with color distributions that are more sim-



Figure 2. Visual comparisons on stroke-based colorization.

ilar and harmonious to their surroundings. To handle more complex and heavy color artifacts caused by the low fidelity characteristics of the diffusion model, we introduce deformable convolution layers [8] into the decoder of SD autoencoder. Guided by the content of the input images, these layers constrain regions of the deformation to align the generated colors to the input textures, consequently reducing issues of low color fidelity, *i.e.*, color overflow and incorrect color.

Moreover, we present a new method to enable stroke-based colorization. In particular, we incorporate combinations of a hint point map, a binary mask, and an input grayscale image into the SD model. The hint points are located using strokes. To indicate the positions of the hint points explicitly, we introduce a binary mask derived from the hint point map. By encoding the hint points into the latent space during the denoising process, we gain control over the denoised color distribution. This allows users to flexibly modify the color of an image using arbitrary strokes, enabling modifications on specific local regions. We leave the details of prompt-based and exemplar-based colorization to the methodology section.

In this study, we present the diverse applications of our method through a preview of our results, as shown in Fig. 1. Our approach offers a versatile and effective solution for implementing highly controllable image colorization, achieving state-of-the-art performance in terms of color richness, stability, and visual quality for image colorization. We also provide a video demo to showcase an interactive interface that demonstrates the multi-modal colorization and local controllability of our method.

To summarize, our main contributions are as follows: 1) We propose a novel diffusion model-based framework, CtrlColor, which enables highly controllable multi-modal colorization. Our framework supports prompt-based, stroke-based, exemplar-based, and a combination of these conditions for local and global colorization. 2) Our approach addresses the color overflow problem by employing training-free self-attention guidance and the learned content-guided deformable autoencoder. 3) We introduce a new approach to add user strokes to control the color locally and precisely by encoding the strokes’ position and color into the diffusion process. 4) Besides overcoming the low fidelity of the pre-trained SD model, our method leverages its advantages, producing colored images that exhibit a richer variation in

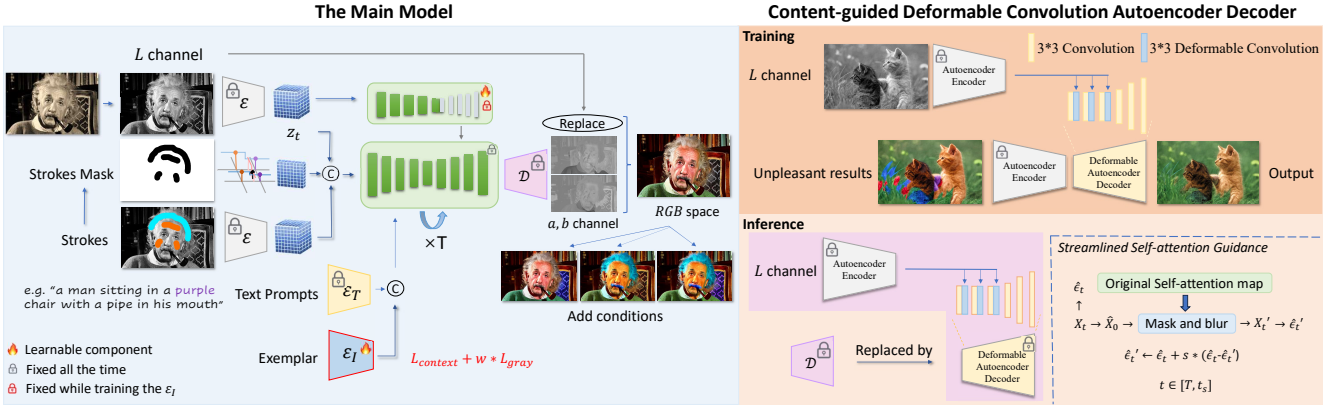


Figure 3. **Left:** The main structure of our CtrlColor Model achieves multi-modal controllable colorization by blending controls from diverse components. **Right:** To manage large color overflow and inaccurate color regions, we integrate content-guided deformable convolution layers into the autoencoder’s decoder. These layers restrict deformed color regions to align with nearby colors. Additionally, refined self-attention guidance is employed during inference to blur small overflow areas by referencing the surrounding color distribution. This process aims to smooth the color distribution, effectively addressing the issue of small color overflow.

color compared to previous methods.

2. Related Work

Unconditional Colorization. Unconditional colorization aims to colorize grayscale images automatically. Early attempts formulate colorization as either a regression [7] or a classification task [54]. To further guide colorization with semantic information, class labels [25], semantic segmentation maps [57], or/and instance bounding box [42] are incorporated into colorization networks. The recent Generative Adversarial Network (GAN) [12] and Transformer [43] have also shown promising results in colorization. DeOldify [1] and ChromaGan [44] directly optimize the GAN-based networks, whereas Wu et al. [47] and Kim et al. [25] exploit the generative prior of the pre-trained GANs. Benefiting from its long-range receptive field, Transformer architecture is used to auto-regressively predict color tokens either in pixel space [26] or in the latent space [20, 23, 48]. More recently, Palette [37] trains a diffusion model from scratch conditioned on grayscale images to generate diverse colors. However, the knowledge of color hint is still restricted to the limited colorization training data, hindering its ability to generate more vivid colors.

Conditional Colorization. Conditional colorization adds user controls to the colorization process. Based on input modality, it can be categorized into three types: stroke-based colorization, exemplar-based colorization, and prompt-based colorization. Prior stroke-based colorization works rely on similarity metrics [28, 31] such as spatial offset or learned through neural networks [10] to propagate local color hints to the whole image. Recent methods use end-to-end propagation frameworks [20, 49, 50]. Exemplar-based colorization works mainly employ a pre-trained network for feature matching between the input grayscale image and the exemplar image [14, 52]. Huang et al. [20] further regulates the matching matrix by converting only cells

with high matching confidence to hint points. Prompt-based colorization takes text descriptions as guidance to assist colorization. One direction revolves around fusing text and image features. Feature-wise affine transformation [32] and recurrent attentive model [6] have been proposed. Some other studies focus on decoupling color and object feature space to avoid color-object mismatch and color-object coupling [46]. More recent works [5, 51] use diffusion prior to achieve prompt control, but the output size of L-CAD [5] is limited and the results of Diffusing Colors [51] suffer from severe color overflow. UniColor [20], leveraging Transformer [43] and VQGAN [11], is a seminal work unifying all three types of conditions by representing them as hint points across fixed-sized cell regions. However, one cell region consists of many pixels, possibly with diverse colors. Simply representing them with one color may lead to undesired results like color bleeding. In contrast, our approach manipulates different conditions in latent space via various encoding approaches and adopts a pixel-level binary mask for strokes, achieving highly precise and flexible control.

Diffusion Models for Image Generation. The diffusion probabilistic model has shown successful results in image generation [9, 17, 41], which is extended to latent space [36] and text conditioned generation [33, 38]. GLIDE [33] and Imagen [38] encode text inputs into latent vectors using pre-trained vision or/and language models like CLIP [34] and T5 [35]. To further enhance control over diffusion models, several methods exploit input mask [3, 33], encoded text features [15, 24] and decompose image into basic control components [19]. Zhang et al. [53] propose ControlNet to control diffusion model with task-specific conditions such as human key points and user scribbles by fine-tuning a “trainable copy” of any off-the-shelf diffusion model. However, training ControlNet naively with grayscale images as conditions generates images with noticeable differences compared to the input, particularly in textures and details, which is undesirable for colorization.

3. Methodology

3.1. Preliminary: LDM and ControlNet

Diffusion Model consists of a forward and a backward process. In the forward process, Gaussian noise is gradually added to the input image \mathbf{x}_0 in T steps, producing a series of noisy samples $\mathbf{x}_1, \dots, \mathbf{x}_T$. When T is large enough, \mathbf{x}_T approximates a Gaussian distribution. In the backward process, a denoising neural network (typically in the form of U-Net) is used to recover \mathbf{x}_0 from \mathbf{x}_T , as shown in Eq. (1). Specifically, in each time step t during the diffusion reverse process, given the latent noised image code X_t , the diffusion model will output the predicted noise ϵ_t , its variance σ_t^2 , and the attention map A_t , and then we use the predicted noise to get X_{t-1} , *i.e.*, the latent noised image code at step $t - 1$. We use the A_t to modify ϵ_t in our streamlined self-attention guidance.

$$\hat{X}_0 = \frac{X_t - \sqrt{1 - \bar{\alpha}_t} \epsilon_t}{\sqrt{\bar{\alpha}_t}}, \quad (1)$$

where $\bar{\alpha}_t = \prod_{i=1}^t (1 - \sigma_i^2)$.

Latent Diffusion Model (LDM). LDM [36] is proposed to run the diffusion process in latent space instead of pixel space, which saves computational costs. LDM introduces an autoencoder model for image reconstruction. The encoder \mathcal{E} encodes the input image into a 2D latent space \mathbf{z} . The decoder \mathcal{D} then reconstructs the image from \mathbf{z} . Thus, the overall LDM framework consists of a denoising network (U-Net) and an autoencoder. Our designs target these two components, as shown in Fig. 3. The overall loss can be expressed as:

$$\mathcal{L}_{LDM} = \mathbb{E}_{\mathcal{E}(\mathbf{x}), y, \epsilon \sim \mathcal{N}(0,1), t} \left[\|\epsilon - \epsilon_\theta(z_t, t)\|_2^2 \right], \quad (2)$$

where t denotes the diffusion step, while ϵ_θ is the denoising network.

ControlNet. ControlNet [53] uses “trainable copy” of LDM on task-specific datasets with an additional input condition c_i apart from the text condition y , while the “locked copy” preserves the original weights of the pre-trained LDM. With these designs, ControlNet achieves more control over generated image content. The overall learning objective then becomes:

$$\mathcal{L} = \mathbb{E}_{\mathcal{E}(\mathbf{x}), y, c_i, \epsilon \sim \mathcal{N}(0,1), t} \left[\|\epsilon - \epsilon_\theta(z_t, t, y, c_i)\|_2^2 \right]. \quad (3)$$

By freezing the parameters of the pre-trained LDM to allow for efficient training, we successfully transfer the generative prior from LDM to image colorization tasks.

3.2. Framework of Control Color

As shown in Fig. 3, our approach consists of two main components: 1) image colorization latent diffusion model

to achieve multi-modal controls; 2) content-guided deformable autoencoder and streamlined self-attention guidance to handle color overflow and incorrect color issues.

3.2.1 Unconditional Colorization

In Fig. 3 (left), we first convert the input image into *Lab* space and get its *L* channel. The *L* channel is first encoded into the latent space using the autoencoder’s encoder, then serves as an extra condition input to ControlNet. The input *RGB* image is also encoded and used as input of the Stable Diffusion model. This operation allows the trained model to generate colored images that closely resemble the structure of the input grayscale image.

Previous methods [23, 54] predict the *ab* channels given the corresponding *L*. We employ a similar strategy, but only in the post-processing, to mitigate the small deformations introduced by the diffusion model while retaining the generated color characteristics. The output is reconstructed by our autoencoder’s decoder and then converted from *RGB* space to *Lab* space. We replace the reconstructed *L* channel with the original input *L* channel and then convert the resulting *Lab* image back to *RGB* space to obtain the final output. This post-processing ensures the final output has the same content as the input.

3.2.2 Conditional Colorization

Based on the above unconditional colorization, we add multi-modal controls by the following designs.

Prompt Control. Consistent with approaches adopted in prior research [36, 53], our methodology involves initially encoding the text prompt using the CLIP [34] text encoder. Subsequently, this encoded information is integrated into the intermediate layers of the U-Net architecture through a cross-attention layer, a process applied within both the ControlNet and Stable Diffusion model frameworks. Leveraging the cross-attention mechanism enables our model to effectively interpret and respond to text prompts, ensuring precise control over the generated content.

Stroke Control. The strokes are first directly overlaid on the *L* channel images, denoted as hint images, so that we can get both the color and the position of the strokes. A binary mask is then derived from the hint image. The input image $I_i \in \mathbb{R}^{C \times H \times W}$ and the hint image $I_s \in \mathbb{R}^{C \times H \times W}$ are encoded into the latent space to get the input latent feature $z_i^{4 \times \frac{H}{8} \times \frac{W}{8}}$ and the hint latent feature $z_s^{4 \times \frac{H}{8} \times \frac{W}{8}}$, respectively. We apply nearest-neighbor downsampling to down-sample the stroke mask to $z_m^{1 \times \frac{H}{8} \times \frac{W}{8}}$. Then we concatenate them into a $\tilde{z}^{9 \times \frac{H}{8} \times \frac{W}{8}} = (z_i, z_m, z_s)$, and feed them to the U-Net structure in the denoising process. We only feed the input grayscale latent feature z_i into the ControlNet component. The objective function then becomes:

$$\mathcal{L} = \mathbb{E}_{\mathcal{E}(\mathbf{x}), y, z_i, \epsilon \sim \mathcal{N}(0,1), t} \left[\|\epsilon - \epsilon_\theta(\tilde{z}_t, t, y, z_i)\|_2^2 \right]. \quad (4)$$

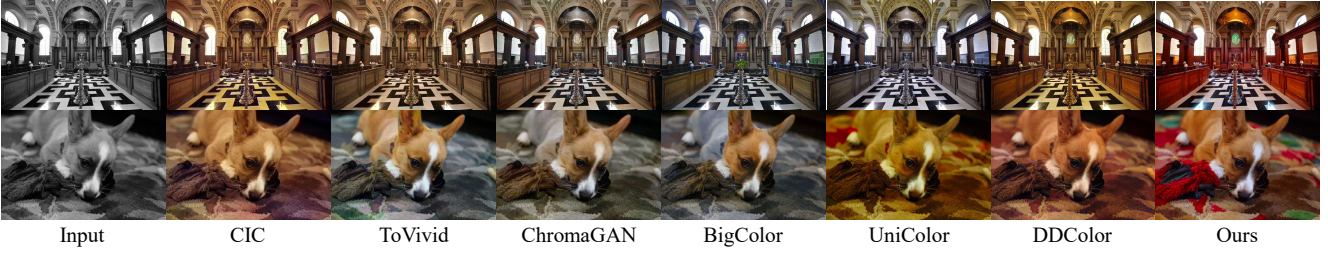


Figure 4. Qualitative comparison for unconditional image colorization. The first row of images is from the COCO-stuff dataset, and the second row comes from the ImageNet validation dataset. Our method generates more vivid and realistic colors with less color bleeding. (**Zoom-in for best view**) More comparisons are provided in the supplementary material.

Exemplar Control. For exemplar-based image colorization, we add a CLIP image encoder to encode exemplars into latent features and feed them into the cross-attention blocks. During training, all the other parts of the model are fixed and only the image encoder is fine-tuned. Since there is no paired data for exemplar-based colorization, inspired by Zhang *et al.* [52], we employ **contextual loss** to constrain color distribution of the generated results similar to the exemplars’.

$$\begin{aligned}
 d^l(i, j) &= \cos(\phi_{I_e}^l(i), \phi_{I_g}^l(j)), \\
 A^l(i, j) &= \underset{j}{\text{softmax}}(1 - \tilde{d}^l(i, j)/h), \\
 L_{\text{context}} &= \sum_{l \in \{3, 5\}} w_l [-\log(\frac{1}{N_l} \sum_i \max_j (A^l(i, j)))] ,
 \end{aligned} \tag{5}$$

where ϕ^l are the l^{th} layers of the pretrained VGG19 model [40], I_e is the exemplar image and I_g is the predicted images at diffusion time step t , formulated in Eq. (7). $\tilde{d}^l(i, j)$ is the normalized cosine similarity $d^l(i, j)$ of pairwise feature points. $A^l(i, j)$ denotes the pairwise affinities between features from l^{th} layer. The parameter h is set to 0.01 and w_l are set to 8, 4, 2 for $l = 5, 4, 3$.

Besides, we introduce a **grayscale loss** to constrain the content of the generated result similar to the input image.

$$L_{\text{gray}} = \left\| \frac{\sum_{\{R, G, B\}} I_i}{3} - \frac{\sum_{\{R, G, B\}} I_g}{3} \right\|_2, \tag{6}$$

where I_i is the input image regenerated by the autoencoder and I_g is the decoded generated result in each diffusion timestep t , which can be formulated as:

$$\begin{aligned}
 I_i &= \Phi_d(\Phi_e(I_{in})), \\
 I_g &= \Phi_d\left(\frac{X_t - \sqrt{1 - \bar{\alpha}_t} \epsilon_t}{\sqrt{\bar{\alpha}_t}}\right),
 \end{aligned} \tag{7}$$

where I_{in} is the original ground truth image, ϵ_t is the predicted noise at time step t , X_t is the latent code of the image at t in the diffusion forward process and Φ_e and Φ_d are the encoder and decoder of the fixed autoencoder. **The final loss function** for training exemplar-based colorization can be formulated as:

$$L_{\text{exemplar}} = L_{\text{context}} + w_e * L_{\text{gray}}. \tag{8}$$

We set w_e to 1000 empirically.

3.2.3 Color Overflow and Incorrect Color Handling

Content-guided Deformable Autoencoder. To handle large color overflow and incorrect color regions, we introduce content-guided deformable convolution layers into the autoencoder’s decoder, as shown in Fig. 3 (right).

Specifically, we add a deformable convolution layer after each of the first three convolution blocks in the decoder of the autoencoder. The input grayscale image $I_i \in \mathbb{R}^{3 \times H \times W}$ is first encoded into the latent space as $z^{4 \times \frac{H}{8} \times \frac{W}{8}}$ using the fixed original autoencoder’s encoder and then fed into the deformable convolution as guidance. During training, we only train these three additional deformable convolution layers. The deformed color images are generated by our main model randomly using different types of conditional colorizations. The loss function is *perceptual loss* for the first 500 training steps to constrain the reconstruction and *perceptual loss* + $0.025 \times \text{discriminator loss}$ for the following steps.

During inference, we replace the original autoencoder’s decoder with the learned deformable-enabled decoder and feed the input grayscale image as guidance to it in the same way as training. In our interface, users have the option to choose whether to employ the learned decoder. The learned decoder tends to align colors within the same area, toward similarity. However, users may opt against its use to retain greater flexibility.

Streamlined Self-Attention Guidance. Inspired by Hong *et al.* [18] for improving sample quality of generative models, we introduce training-free guidance in the inference process to handle small color overflow, as shown in Fig. 3 (bottom right). This refined self-attention guidance is employed during inference to blur and re-predict small overflow areas by referencing the surrounding color distribution.

In particular, we modify the predicted noise ϵ_t using the following steps. The attention map A_t is the similarity map calculated by the query Q and the key K after softmax in each attention block. We follow [18] to get the degraded predicted \hat{X}_0' and the attention mask M_t , which masks out the majority of the image except for salient parts.

To better retain the original color distribution, different from Hong *et al.* [18], we preserve the degraded \hat{X}_0' without additional noise to retain more unmasked color information. Specifically, we obtain X_t' from Eq. (9) and the modified $\hat{\epsilon}_t'$ from Eq. (11). Then for $t \in [T, t_s]$, we use $\hat{\epsilon}_t'$ from Eq. (11)

to replace $\hat{\epsilon}_t$ and output the new predicted X_{t-1} . Here the number of the total denoising steps T is 1000 and we set t_s to 600 empirically.

$$X'_t \leftarrow (1 - M_t) \odot X'_t + M_t \odot \hat{X}'_t, \quad (9)$$

$$\hat{\epsilon}'_t \leftarrow model(X'_t), \quad (10)$$

$$\hat{\epsilon}'_t \leftarrow \hat{\epsilon}_t + s * (\hat{\epsilon}_t - \hat{\epsilon}'_t), \quad (11)$$

where \odot represents element-wise multiplication, $model$ represents our diffusion model and s denotes the scale of the guidance. Based on experiments, we set s to 0.05. We offer an option to change s in our interface. Further discussion on the impact of s is provided in our suppl..

4. Experiments

4.1. Implementation

Training. We implement our method with PyTorch and train it on four NVIDIA RTX 3090Ti GPUs. We use AdamW optimizer with $\beta_1 = 0.9$ and $\beta_2 = 0.999$. The learning rate is set to 10^{-5} . We train our model for 80K global steps with a batch size of 64. The first 15K training is based on the Stable Diffusion v1.5 and the later 65K global steps add the stroke branch as shown in Fig. 3 for further finetuning. Following Stable Diffusion [36], we resize the input images to 512×512 and convert them to *Lab* color space, and use the *L* channel as the input condition. For exemplar-based colorization, we train the image encoder for 100K global steps. For the deformable convolution layers training, we train it for 9K global steps.

To make the model more sensitive to color, we collect a dictionary of 235 commonly used English words that describe colors for filtering. During the training process, we generate all the captions automatically using BLIP [29]. If a generated caption does not describe a black-and-white image (*i.e.*, does not include phrases like “a black and white photo of \dots ”), and contains color-related words, we reserve all these captions as input. For the remaining captions, we randomly make 60% of them to be empty, which are used for training the unconditional generation.

To simulate both the spontaneous strokes of users and the presence of more hints in exemplars, we first utilize Simple Linear Iterative Clustering (SLIC) [2] to obtain a superpixel representation of the image. Then for each image, we randomly crop 1 to 100 areas that are rectangular regions of varying sizes from 5×5 to 50×50 pixels. There is a 20% probability that these regions correspond to local regions from the ground truth, while the remaining 80% are local regions from the superpixel representation. In addition, we apply color jittering to 20% of the hint images and ground truth. The purpose is to guide our model to trust the hint points rather than just output normal color distribution regardless of whether hints are given. At this stage, the hint images are always non-empty, while the prompt input

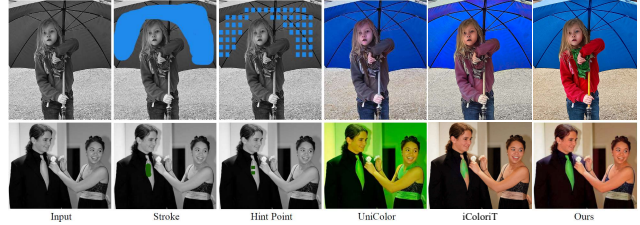


Figure 5. Qualitative comparisons on stroke-based colorization.



Figure 6. Qualitative comparisons on prompt-based colorization.

is always empty, ensuring that the model can still generate normal-colored images during the prompt-based conditional generation process.

Inference. We use a single NVIDIA RTX 3090Ti GPU for inference. Since the diffusion model is trained on the images of size 512×512 and is sensitive to the resolutions, we proportionally resize the input image to a shorter side of 512 pixels before feeding it to our model. Then, we resize it back to its original size before replacing the *L* channel.

4.2. Dataset

Training Data. For training of unconditional, prompt-based, and stroke-based colorization, we use the ImageNet training dataset and filter out relatively gray images. Specifically, we calculate the mean of the variance of the difference between every two channels of the RGB images, denoted as $E(Var(C_i, C_j))$, and filter out the images whose $E(Var(C_i, C_j))$ is lower than a threshold. We set the

Table 1. Quantitative results for unconditional colorization on the ImageNet val5k dataset, ImageNet ctest dataset, and COCO-Stuff dataset. “Ours” is purely unconditional. As for “Ours (hint)”, we randomly give 50-100 random hint points for each image (each image has more than 260K pixels). Results indicate the inherent color priors in our model are more colorful than ImageNet and the effectiveness of our stroke-based colorization.

Dataset Metrics	ImageNet (val5k)		ImageNet (ctest)		COCO-Stuff	
	FID↓	Colorfulness↑	FID↓	Colorfulness↑	FID↓	Colorfulness↑
CIC [54]	22.0860	37.0313	12.7651	37.5761	33.3418	37.6487
UGColor [55]	15.1777	27.0966	6.5466	27.8122	21.4010	28.4487
DeOldify [1]	10.5191	26.4827	4.2143	23.1538	13.4318	28.3779
ChromaGAN [44]	16.4390	25.5862	9.3487	29.0895	26.4624	29.1411
InstColor [42]	12.9455	27.5710	6.7803	28.1923	12.6844	29.2302
ToVivid [47]	5.8019	37.3376	2.6775	37.8425	8.5452	38.8155
BigColor [25]	7.7677	42.5364	2.8583	44.4135	10.0362	43.4104
DISCO [48]	10.2895	40.9533	5.7196	37.4613	13.3850	39.1969
DDColor [23]	5.5726	42.8370	2.6294	42.9575	7.2718	42.2919
ColorFormer [22]	6.3831	40.5631	2.9816	41.2833	8.5623	41.0248
UniColor [20]	9.6292	36.3415	4.9140	37.1726	8.0509	36.7442
Ours	8.8749	47.1680	4.2915	44.9256	10.2651	47.0501
Ours (hint)	4.6657	32.3621	2.0990	33.5493	6.8830	32.0113



Figure 7. Visual examples for our stroke-based colorization.

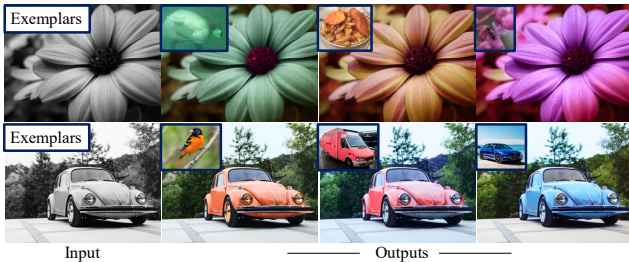


Figure 8. Visual examples for our exemplar-based colorization.

threshold to 12 empirically.

For exemplar-based colorization training, we use the same ImageNet data as the inputs. Because we aim to colorize target images based on semantically similar objects in the exemplars, we utilize CLIP [34] for corresponding exemplar retrieval. Specifically, we first use the pre-trained CLIP image encoder to get the features of each image in the dataset, then for each input image, we traverse through the features of all the other images in the same class as itself, calculate the cosine similarity between the feature of the given picture and other pictures, and then select the image with the highest similarity as the exemplar for that image.

For content-guided deformable convolution decoder training, we randomly select 100K images from ImageNet training dataset and use 30% exemplar-based colorization and 70% other types of our colorization methods to generate the images as the deformed color images to train.

Evaluation Data. For unconditional image colorization, following [23], we perform evaluations on the whole COCO-stuff validation set [4] and the first 5k images in ImageNet validation dataset, *i.e.*, val5k, and following [27], we also perform evaluations on the ImageNet ctest dataset (10k images), another subset of the ImageNet validation set. For prompt-based image colorization, following Weng *et al.* [46], we use the COCO-Stuff validation set [4] and keep only images with adjectives in captions (2.4k images).

4.3. Comparisons

For fair comparisons, we only compare our method with state-of-the-art methods that keep input and output resolutions unchanged. For image colorization, following Huang *et al.* [20], we use Fréchet Inception Distance (FID) [16] and colorfulness [13] for unconditional and prompt-based colorization. For prompt-based methods, we also employ the CLIP score [34] to evaluate the proximity between colorized images and text descriptions in the CLIP latent space.

Unconditional Colorization Comparison. For unconditional colorization, we compare our method with two types of state-of-the-art methods: 1) six CNN-based methods: CIC [54], UGColor [55], DeOldify [1], ChromaGAN [44], InstColor [42], ToVivid [47], and BigColor [25]; 2) four Transformer-based methods: UniColor [20], DISCO [48], ColorFormer [22], and DDColor [23].

For quantitative comparison, as presented in Tab. 1, our pure unconditional colorization achieves state-of-the-art performance in terms of colorfulness yet FID. This suggests our unconditional method generates more colorful results but the color distribution may be different from the ImageNet dataset, due to the SD model pre-trained on LAION-5B [39], which is more colorful and high-quality than ImageNet. But with hints from ImageNet added, our method can achieve top performance in terms of FID but colorfulness becomes low. The results show that by providing some reasonable hints, our method achieves a color distribution closest to the ground truth, showing the effectiveness of our stroke-based colorization. This also indicates that ImageNet images are less colorful than the color priors in our model.

We show the visual comparison with state-of-the-art methods in Fig. 4. As shown, while the compared methods tend to generate brown and greyish images, our method generates vivid and realistic colors with less color overflow.

Stroke-based Colorization Comparison. We compare visual results among our method, UniColor [20], and iColoriT [50] with manually drawn strokes in Fig. 5. Our method can generate vivid and plausible colors outside the drawn object (*e.g.*, the girl holding umbrella in the 1st row). When the stroke is localized on a small object, our method achieves localized colorization without altering global hue (*e.g.*, green stroke drawn on the man’s tie in the 2nd row). Fig. 7 showcases more results on stroke-based colorization.

Prompt-based Colorization Comparison. We compare our method with UniColor [20], L-CAD [5] and UniColor [20] are the only two methods with publicly available code for prompt-based colorization, but the output size of L-CAD [5] is 256×256 , so we do not compare it for fairness.

Table 2. Quantitative results for prompt-based colorization on COCO-Stuff [4] dataset.

	FID↓	Colorfulness↑	CLIP score↑
UniColor [20]	16.6911	45.7293	0.7649
Ours	15.2651	65.5266	0.7871



Figure 9. The ablation study for content-guided deformable autoencoder decoder and streamlined self-attention guidance (SAG). The output without SAG and the deformable layers will generate incorrect colors in small objects, like the shadow, scarf, arms, hat, and so on.

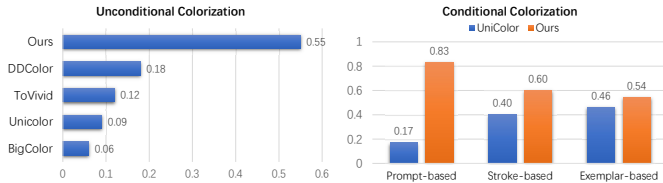


Figure 10. Quantitative results of our user study.

Quantitatively, as shown in Tab. 2, our method achieves better FID, Colorfulness, and CLIP scores than those of UniColor, suggesting that our results are closer to the ground truth images given the color-description captions and have better alignment with the given captions. We also show the visual comparison in Fig. 6. Our method colorizes images with more vivid colors and better color consistency.

Exemplar-based Colorization Showcase. We show some visual examples in Fig. 8. Overall, our method can colorize the inputs with a similar color distribution to exemplars while keeping the color realistic and visually pleasant.

4.4. User Study

Since colorization algorithms are mainly applied in the field of creative arts and old photo restoration, human satisfaction is always a more reasonable indicator of the algorithm’s performance. We conduct a user study to further show the superior performance of our method. Our study is divided into four sections corresponding to unconditional, prompt-based, stroke-based, and exemplar-based colorization, respectively. Each section consists of 10 questions. In each question, participants are asked to select the *best* image among several compared methods. We define *best* based on the following metrics: perceptual realism (less color overflow), color richness, aesthetic sense, and faithful reconstruction given the input condition (if available). We select DDColor [23], ToVivid [47], BigColor [25], and UniColor [20] for unconditional colorization, and UniColor [20] for three condition-based colorization. We obtain 33 valid responses for unconditional colorization and 41 valid responses for conditional colorization. The statistic is shown in Fig. 10. Our method outperforms all the other methods.

4.5. Ablation Study

We carry out ablation studies to further analyze our designs. **The impact of stroke numbers.** We conduct a quantitative

Table 3. The impact of the number of strokes.

number of cropped cells	FID↓	Colorfulness↑	PSNR↑	SSIM↑	LPIPS↓
0 - 20	8.8614	36.3481	24.4910	0.9918	0.1305
20-50	7.8182	32.9553	26.6695	0.9924	0.1034
50 - 100	6.8830	32.0113	28.2699	0.9926	0.0872

study on the COCO-stuff dataset with randomly selected 16×16 cell regions. The color of the hints is derived from the mean of the superpixels in the region. As shown in Tab. 3, the more strokes are (as reflected by the number of cells), the closer the colorized image is to ground truth as reflected by the FID, PSNR [21], SSIM [45], and LPIPS [56] values. There is also a trade-off between image colorfulness and faithful color reconstruction given stroke colors, as more stroked regions mean less space left to exploit the rich color priors in our model.

The effectiveness of content-guided deformable convolution layer and streamlined self-attention guidance. As shown in Fig. 9, in the original results, objects are miscolored when segmented, shadows are also incorrectly colored, and there is slight color overflow. For example, in the first row, the lower part of the woman’s scarf is white, but the upper part is colored blue; the dog’s neck, legs, and the person’s arms have small areas of miscoloring or overflow. In the second row, shadows are colored red, there’s bleeding on the bag, and inconsistency on the hat, where the brim is red while the top is brown. After adding streamlined self-attention guidance, minor bleeding or miscoloring in small areas was fixed. Moreover, using the deformable decoder unifies the colors of the same object and corrects large-region miscoloring.

5. Conclusion

In this paper, we successfully achieve highly controllable multi-modal image colorization. Our method is built on a pre-trained SD model with new designs such as stroke control and exemplar control, which offer a diverse range of colors and high user interactivity. With our content-guided deformable convolution autoencoder decoder and streamlined self-attention guidance, we effectively mitigate color overflow and miscoloring. Our study is an early attempt to employ SD model to handle multi-control colorization and deal with miscoloring. We believe our work can provide significant insights into controllable image colorization.

References

- [1] Deoldify. <https://github.com/jantic/DeOldify>, 2019. 3, 6, 7
- [2] Radhakrishna Achanta, Appu Shaji, Kevin Smith, Aurelien Lucchi, Pascal Fua, and Sabine Süsstrunk. Slic superpixels compared to state-of-the-art superpixel methods. *IEEE TPAMI*, 2012. 6
- [3] Omri Avrahami, Dani Lischinski, and Ohad Fried. Blended diffusion for text-driven editing of natural images. In *CVPR*, 2022. 3
- [4] Holger Caesar, Jasper Uijlings, and Vittorio Ferrari. Cocostuff: Thing and stuff classes in context. In *CVPR*, 2018. 7
- [5] Zheng Chang, Shuchen Weng, Peixuan Zhang, Yu Li, Si Li, and Boxin Shi. L-cad: Language-based colorization with any-level descriptions. *NeurIPS*, 2023. 3, 7
- [6] Jianbo Chen, Yelong Shen, Jianfeng Gao, Jingjing Liu, and Xiaodong Liu. Language-based image editing with recurrent attentive models. In *CVPR*, 2018. 3
- [7] Zezhou Cheng, Qingxiong Yang, and Bin Sheng. Deep colorization. In *ICCV*, 2015. 2, 3
- [8] Jifeng Dai, Haozhi Qi, Yuwen Xiong, Yi Li, Guodong Zhang, Han Hu, and Yichen Wei. Deformable convolutional networks. In *ICCV*, 2017. 2
- [9] Prafulla Dhariwal and Alexander Nichol. Diffusion models beat gans on image synthesis. 2021. 3
- [10] Yuki Endo, Satoshi Iizuka, Yoshihiro Kanamori, and Jun Mitani. Deepprop: Extracting deep features from a single image for edit propagation. In *Computer Graphics Forum*, 2016. 3
- [11] Patrick Esser, Robin Rombach, and Bjorn Ommer. Taming transformers for high-resolution image synthesis. In *CVPR*, 2021. 3
- [12] Ian Goodfellow, Jean Pouget-Abadie, Mehdi Mirza, Bing Xu, David Warde-Farley, Sherjil Ozair, Aaron Courville, and Yoshua Bengio. Generative adversarial networks. *Communications of the ACM*, 2020. 3
- [13] David Hasler and Sabine E Suesstrunk. Measuring colorfulness in natural images. In *Human vision and electronic imaging VIII*, 2003. 7
- [14] Mingming He, Dongdong Chen, Jing Liao, Pedro V Sander, and Lu Yuan. Deep exemplar-based colorization. *ACM Transactions on Graphics (TOG)*, 2018. 3
- [15] Amir Hertz, Ron Mokady, Jay Tenenbaum, Kfir Aberman, Yael Pritch, and Daniel Cohen-Or. Prompt-to-prompt image editing with cross attention control. *arXiv preprint arXiv:2208.01626*, 2022. 3
- [16] Martin Heusel, Hubert Ramsauer, Thomas Unterthiner, Bernhard Nessler, and Sepp Hochreiter. Gans trained by a two time-scale update rule converge to a local nash equilibrium. 2017. 7
- [17] Jonathan Ho, Ajay Jain, and Pieter Abbeel. Denoising diffusion probabilistic models. *NeurIPS*, 2020. 3
- [18] Susung Hong, Gyuseong Lee, Wooseok Jang, and Seungryong Kim. Improving sample quality of diffusion models using self-attention guidance. In *ICCV*, 2023. 5
- [19] Lianghua Huang, Di Chen, Yu Liu, Yujun Shen, Deli Zhao, and Jingren Zhou. Composer: Creative and controllable image synthesis with composable conditions. *arXiv preprint arXiv:2302.09778*, 2023. 3
- [20] Zhitong Huang, Nanxuan Zhao, and Jing Liao. Unicolor: A unified framework for multi-modal colorization with transformer. *ACM Transactions on Graphics (TOG)*, 2022. 2, 3, 6, 7, 8, 16
- [21] Quan Huynh-Thu and Mohammed Ghanbari. Scope of validity of psnr in image/video quality assessment. *Electronics letters*, 2008. 8
- [22] Xiaozhong Ji, Boyuan Jiang, Donghao Luo, Guangpin Tao, Wenqing Chu, Zhifeng Xie, Chengjie Wang, and Ying Tai. Colorformer: Image colorization via color memory assisted hybrid-attention transformer. In *ECCV*, 2022. 6, 7
- [23] Xiaoyang Kang, Tao Yang, Wenqi Ouyang, Peiran Ren, Lingzhi Li, and Xuansong Xie. Ddcolor: Towards photorealistic image colorization via dual decoders. In *ICCV*, 2023. 3, 4, 6, 7, 8
- [24] Bahjat Kawar, Shiran Zada, Oran Lang, Omer Tov, Huiwen Chang, Tali Dekel, Inbar Mosseri, and Michal Irani. Imagic: Text-based real image editing with diffusion models. In *CVPR*, 2023. 3
- [25] Geonung Kim, Kyoungkook Kang, Seongtae Kim, Hwayoon Lee, Sehoon Kim, Jonghyun Kim, Seung-Hwan Baek, and Sunghyun Cho. Bigcolor: Colorization using a generative color prior for natural images. In *ECCV*, 2022. 2, 3, 6, 7, 8
- [26] Manoj Kumar, Dirk Weissenborn, and Nal Kalchbrenner. Colorization transformer. In *ICLR*, 2021. 2, 3
- [27] Gustav Larsson, Michael Maire, and Gregory Shakhnarovich. Learning representations for automatic colorization. In *ECCV*, 2016. 7
- [28] Anat Levin, Dani Lischinski, and Yair Weiss. Colorization using optimization. In *ACM SIGGRAPH 2004 Papers*. 2004. 3
- [29] Junnan Li, Dongxu Li, Caiming Xiong, and Steven Hoi. Blip: Bootstrapping language-image pre-training for unified vision-language understanding and generation. In *ICML*, 2022. 6
- [30] Philipp Lindenberger, Paul-Edouard Sarlin, and Marc Pollefeys. Lightglue: Local feature matching at light speed. In *ICCV*, 2023. 12
- [31] Qing Luan, Fang Wen, Daniel Cohen-Or, Lin Liang, Ying-Qing Xu, and Heung-Yeung Shum. Natural image colorization. In *Proceedings of the 18th Eurographics conference on Rendering Techniques*, 2007. 3
- [32] Varun Manjunatha, Mohit Iyyer, Jordan Boyd-Graber, and Larry Davis. Learning to color from language. In *North American Chapter of the Association for Computational Linguistics*, 2018. 3
- [33] Alex Nichol, Prafulla Dhariwal, Aditya Ramesh, Pranav Shyam, Pamela Mishkin, Bob McGrew, Ilya Sutskever, and Mark Chen. Glide: Towards photorealistic image generation and editing with text-guided diffusion models. *arXiv preprint arXiv:2112.10741*, 2021. 3
- [34] Alec Radford, Jong Wook Kim, Chris Hallacy, Aditya Ramesh, Gabriel Goh, Sandhini Agarwal, Girish Sastry,

- Amanda Askell, Pamela Mishkin, Jack Clark, et al. Learning transferable visual models from natural language supervision. In *ICML*, 2021. 3, 4, 7
- [35] Colin Raffel, Noam Shazeer, Adam Roberts, Katherine Lee, Sharan Narang, Michael Matena, Yanqi Zhou, Wei Li, and Peter J Liu. Exploring the limits of transfer learning with a unified text-to-text transformer. *The Journal of Machine Learning Research*, 2020. 3
- [36] Robin Rombach, Andreas Blattmann, Dominik Lorenz, Patrick Esser, and Björn Ommer. High-resolution image synthesis with latent diffusion models. In *CVPR*, 2022. 2, 3, 4, 6
- [37] Chitwan Saharia, William Chan, Huiwen Chang, Chris Lee, Jonathan Ho, Tim Salimans, David Fleet, and Mohammad Norouzi. Palette: Image-to-image diffusion models. In *ACM SIGGRAPH 2022 Conference Proceedings*, 2022. 2, 3
- [38] Chitwan Saharia, William Chan, Saurabh Saxena, Lala Li, Jay Whang, Emily L Denton, Kamyar Ghasemipour, Raphael Gontijo Lopes, Burcu Karagol Ayan, Tim Salimans, et al. Photorealistic text-to-image diffusion models with deep language understanding. *NeurIPS*, 2022. 3
- [39] Christoph Schuhmann, Romain Beaumont, Richard Vencu, Cade Gordon, Ross Wightman, Mehdi Cherti, Theo Coombes, Aarush Katta, Clayton Mullis, Mitchell Wortsman, et al. Laion-5b: An open large-scale dataset for training next generation image-text models. *NeurIPS*, 2022. 7
- [40] Karen Simonyan and Andrew Zisserman. Very deep convolutional networks for large-scale image recognition. *arXiv preprint arXiv:1409.1556*, 2014. 5
- [41] Jiaming Song, Chenlin Meng, and Stefano Ermon. Denoising diffusion implicit models. *arXiv preprint arXiv:2010.02502*, 2020. 3
- [42] Jheng-Wei Su, Hung-Kuo Chu, and Jia-Bin Huang. Instance-aware image colorization. In *CVPR*, 2020. 2, 3, 6, 7
- [43] Ashish Vaswani, Noam Shazeer, Niki Parmar, Jakob Uszkoreit, Llion Jones, Aidan N Gomez, Łukasz Kaiser, and Illia Polosukhin. Attention is all you need. *NeurIPS*, 2017. 3
- [44] Patricia Vitoria, Lara Raad, and Coloma Ballester. Chromagan: Adversarial picture colorization with semantic class distribution. In *WACV*, 2020. 2, 3, 6, 7
- [45] Zhou Wang, Alan C Bovik, Hamid R Sheikh, and Eero P Simoncelli. Image quality assessment: from error visibility to structural similarity. *IEEE Transactions on Image Processing*, 2004. 8
- [46] Shuchen Weng, Hao Wu, Zheng Chang, Jiajun Tang, Si Li, and Boxin Shi. L-code: language-based colorization using color-object decoupled conditions. In *AAAI*, 2022. 3, 7
- [47] Yanze Wu, Xintao Wang, Yu Li, Honglun Zhang, Xun Zhao, and Ying Shan. Towards vivid and diverse image colorization with generative color prior. In *ICCV*, 2021. 2, 3, 6, 7, 8
- [48] Menghan Xia, Wenbo Hu, Tien-Tsin Wong, and Jue Wang. Disentangled image colorization via global anchors. *ACM Transactions on Graphics (TOG)*, 2022. 3, 6, 7
- [49] Yi Xiao, Peiyao Zhou, Yan Zheng, and Chi-Sing Leung. Interactive deep colorization using simultaneous global and local inputs. In *ICASSP*, 2019. 3
- [50] Jooyeol Yun, Sanghyeon Lee, Minho Park, and Jaegul Choo. icolorit: Towards propagating local hints to the right region in interactive colorization by leveraging vision transformer. In *WACV*, 2023. 2, 3, 7
- [51] Nir Zabari, Aharon Azulay, Alexey Gorkor, Tavi Halperin, and Ohad Fried. Diffusing colors: Image colorization with text guided diffusion. In *SIGGRAPH Asia 2023*, pages 1–11, 2023. 3
- [52] Bo Zhang, Mingming He, Jing Liao, Pedro V Sander, Lu Yuan, Amine Bermak, and Dong Chen. Deep exemplar-based video colorization. In *CVPR*, 2019. 3, 5
- [53] Lvmin Zhang, Anyi Rao, and Maneesh Agrawala. Adding conditional control to text-to-image diffusion models. In *ICCV*, 2023. 2, 3, 4
- [54] Richard Zhang, Phillip Isola, and Alexei A Efros. Colorful image colorization. In *ECCV*, 2016. 2, 3, 4, 6, 7
- [55] Richard Zhang, Jun-Yan Zhu, Phillip Isola, Xinyang Geng, Angela S Lin, Tianhe Yu, and Alexei A Efros. Real-time user-guided image colorization with learned deep priors. *ACM Transactions on Graphics (TOG)*, 2017. 6, 7
- [56] Richard Zhang, Phillip Isola, Alexei A Efros, Eli Shechtman, and Oliver Wang. The unreasonable effectiveness of deep features as a perceptual metric. In *CVPR*, 2018. 8
- [57] Jiaojiao Zhao, Jungong Han, Ling Shao, and Cees GM Snoek. Pixelated semantic colorization. *International Journal of Computer Vision*, 2020. 2, 3

Control Color: Multimodal Diffusion-based Interactive Image Colorization

Supplementary Material

In this supplementary material, we present various applications of our method (Sec. 6), more ablation studies (Sec. 8), more comparisons (Sec. 9), more results (Sec. 10), the reproducibility explanation (Sec. 11), and the limitations of our approach (Sec. 12). In addition, a video demo is provided to showcase the interactive interface and the effectiveness and high controllability of our method at <https://youtu.be/tSCwA-srl8Q>.

6. Applications

6.1. Interactive Interface

As shown in Fig. 11, we implement the interactive interface of our method using Gradio. The user first provides the image that needs to be colorized at (1), then just clicks the button (2) before any other steps. The user can flexibly give text prompts at (3), draw strokes using (10), or give exemplar at (7). By choosing option (4), the image can be colorized according to the strokes' color, otherwise, it will be colorized unconditionally. By choosing option (5), only the color of the strokes covered areas is changed, otherwise, the whole image is re-colored. To be noted, by choosing both options (4) and (5), our method colorizes the strokes covered areas according to the color of the strokes while colorizing the covered areas unconditionally if one only chooses option (5). By choosing option (6), the original autoencoder will be replaced by a content-guided deformable autoencoder and the latent outputs will be decoded by the learned content-guided deformable autoencoder's decoder, otherwise, the latent denoised outputs will be decoded by the original autoencoder's decoder. Option (4) is True, op-

tion (5) is False, and option (6) is True by default.

The screenshot of the advanced options is shown at the right of Fig. 11. Slider (11) is for changing the quantity of outputs generated each time. The guidance scale of the conditions and the global seed can be changed using the sliders (12) and (15). Increasing the guidance scale leads to higher saturation in the color of the outputs, as shown in Fig. 13. The sliders (13) and (14) are designed to change the control strength of the streamlined self-attention guidance (SAG). SAG scale (13) is the guidance scale of the SAG, and the range $[0.05, 0.15]$ is recommended based on our experiments. (14) is the t_s of Fig. 2 (bottom right) in our main paper. We only change the \hat{e}_t between time step $t \in [T, t_s]$ during inference, and the range $[400, 600]$ is recommended. The parameters of the advanced options in Fig. 11 are the default settings, except for the seed which is randomly initialized.

After setting all the conditions and options, the final results will be shown in (9) after clicking the button at (8).

6.2. Multi Controls Colorization

As shown in Fig. 1 in our main paper and Fig. 16 in this supplementary material, our method supports a mix of text prompts, strokes, and exemplar controls. Our method trusts the strokes most to keep the high and precise controllability because our framework structure always keeps the latent code of the masked regions the same as the input strokes.

6.3. Recolorization

Since our model only takes the L channel as its input, it can recolorize color images in the same manner as it does with

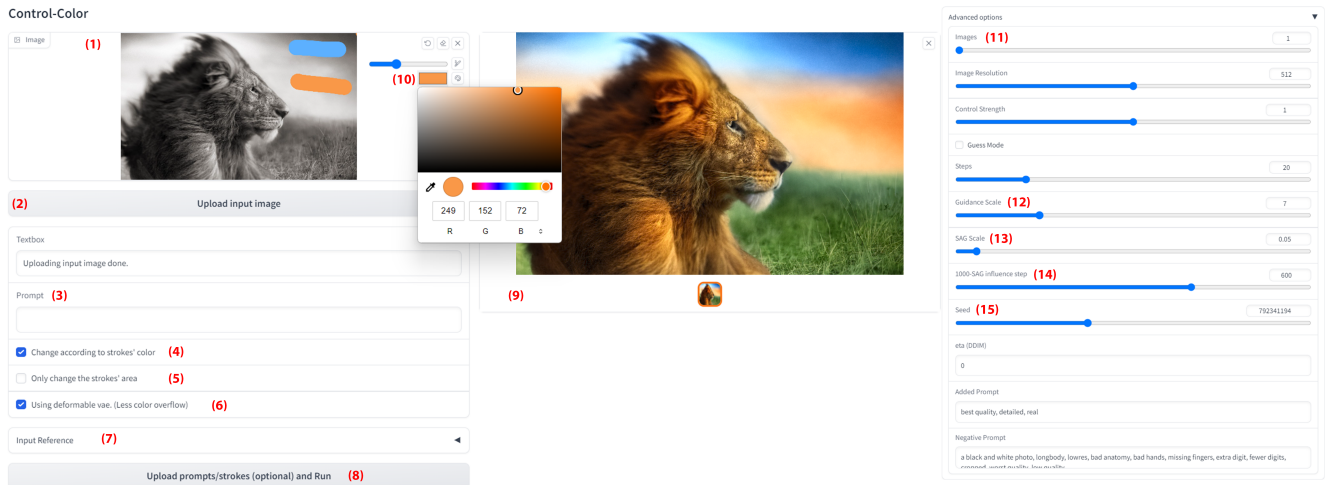


Figure 11. The interactive interface of our CtrlColor. Check out Sec. 6.1 for more details.

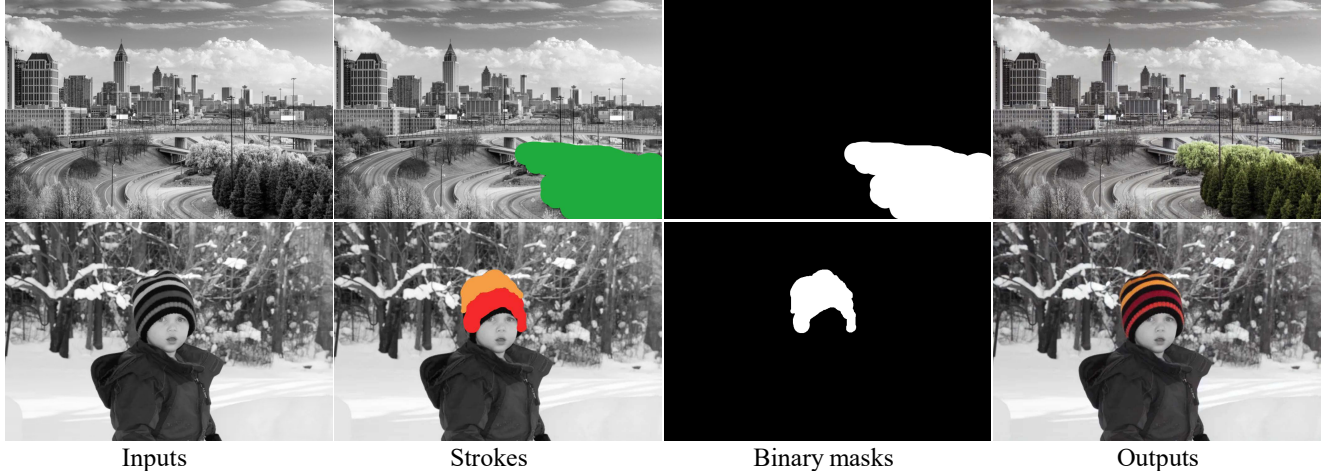


Figure 12. Showcase of our conditional region colorization. For conditional colorization, we input both the color of the strokes and the masks into our model.

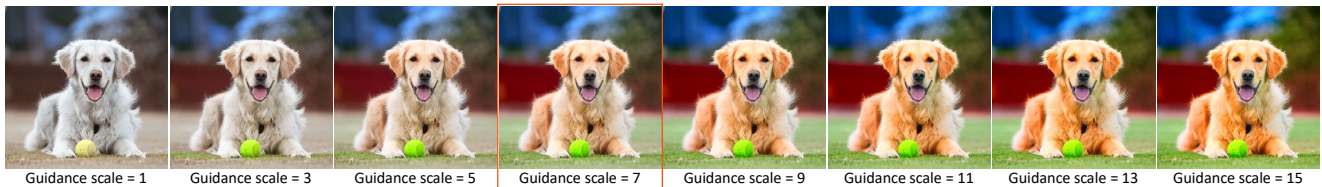


Figure 13. The impact of the guidance scale. The higher the guidance scale, the more saturated the outputs. In our experiments, we set this scale to 7. We offer the option in our interface to let users adjust the saturation of the outputs based on their taste.

grayscale images, as shown in Fig. 16.

6.4. Local Region Colorization

Our method can colorize only part of the input image while keeping the other areas the same as the input. This is achieved by the design of our stroked control approach, specifically, by giving the inverse binary mask as the strokes' mask and giving the unmasked area as the hints, as shown in Figs. 12 and 15 and our video demo.

6.5. Iterative Image Editing

With the same seed, users can easily obtain stable results. Users can also modify the result by adding strokes to it. As shown in our video demo, we can iteratively edit the image by adding different conditions. To be noted, the strokes can be covered by new strokes. Moreover, the text prompts can also be changed during editing.

6.6. Video Colorization

Our methods can easily be extended to video colorization using the feature-matching method, such as Light-GLUE [30], to propagate the first frame to the whole video. We provide some results in the video demo.

7. More Explanations on Key Designs

The inherent characteristic of the diffusion model is to regenerate the content details of an image. These deformations manifest in the final coloring as incorrect color or color overflow problems.

We use the streamlined SAG model to solve the small color overflow problem. The mask obtained from SAG can distinguish between high and low-frequency details, with high-frequency details (such as edges) being prone to deformation, leading to areas of color overflow. We utilize this mask to blur out these high-frequency details and re-predict them according to the surrounding color distribution, as shown in Fig. 17, thereby improving the small color overflow and incorrect color areas caused by the small deformations.

However, the training-free approach may not solve it completely and there are more common and larger mis-coloring problems, such as incorrect color caused by the mirror reflection or the object divided into two separate



Figure 14. The effectiveness of the deformable layers.



Figure 15. Showcase of our unconditional region colorization. For unconditional region colorization, we do not input the strokes' color while only taking the masks as the conditions.

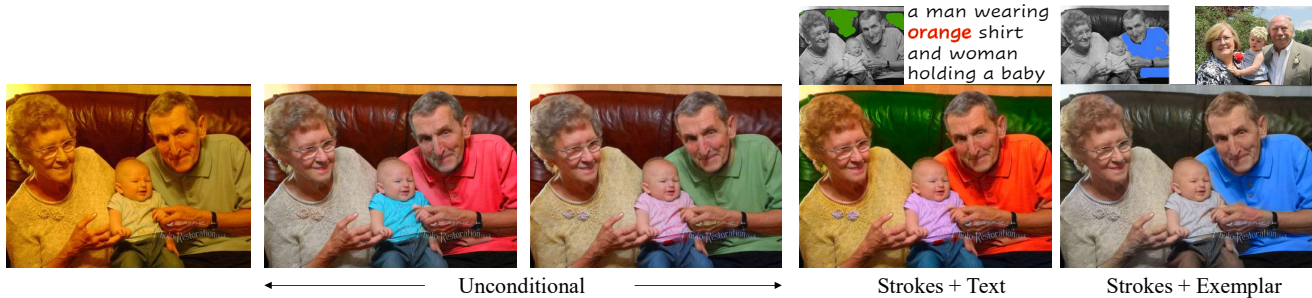


Figure 16. Recolorization and multi controls colorization.

pieces by another object. Thus, we introduce the learnable content-guided deformable layers to correct the larger incorrect color regions. The deformable convolution layer learns an offset according to the given content, allowing the layer to perceive a larger range of features. Consequently, it corrects deformations and inaccurate color regions based on the surrounding color distribution and content. We leverage it to learn and correct inaccurate information, ensuring

consistency in color with the surrounding areas. As shown in Fig. 14, this approach further addresses more severe incorrect color and color overflow issues.

8. More Ablation Studies

Difference from the original SAG. After blurring unmasked areas in \hat{X}_0 , we preserve the degraded \hat{X}_0 without

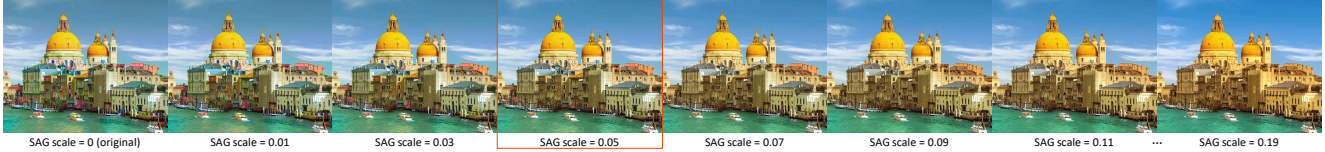


Figure 17. The impact of the SAG scale. Here, all the t_s are set to 600. The original output (the leftmost one) has many color overflow regions on small objects. The output with a large SAG scale (e.g. the rightmost one) tends to colorize large contiguous areas with the same color. Thus, we choose a scale value that effectively eliminates color bleeding without excessively blending the colors, i.e. $s = 0.05$.

Table 4. The comparison between original and streamlined SAG on ImageNet val5k dataset.

SAG type	Colorfulness \uparrow	PSNR \uparrow	SSIM \uparrow	LPIPS \downarrow
original	47.1347	21.0038	0.9873	0.1946
streamlined	47.1680	21.0409	0.9873	0.1946

Table 5. The impact of the self-attention guidance and the deformable convolution layers, tested on ImageNet val5k dataset.

	w/ SAG	w/ Deformable layers	FID \downarrow	Colorfulness \uparrow	PSNR \uparrow	SSIM \uparrow	LPIPS \downarrow
Unconditional			9.7989	59.8463	19.4400	0.9789	0.2414
	✓		11.2395	61.2139	19.3985	0.9810	0.2332
		✓	8.3047	28.6752	21.5241	0.9870	0.1873
Stroke-based			8.8749	47.1680	21.0409	0.9873	0.1946
	✓		5.2778	37.4117	26.6739	0.9887	0.1007
		✓	5.3082	38.6502	27.6023	0.9901	0.0911
	✓	✓	5.0103	28.6752	27.7384	0.9908	0.0927
		✓	4.6657	32.3621	28.4350	0.9914	0.0876

additional noise to retain more unmasked color information, which is the key difference from the original SAG [2]. As shown in Tab. 4, our refined SAG outperforms the original one in most of the metrics. This indicates our streamlined SAG can keep the original color distribution better than the original SAG.

Effectiveness of Self-Attention Guidance and Content-guided Deformable Convolution Autoencoder. The quantitative comparisons in Tab. 5 show that under the same conditions, with the self-attention guidance and the deformable convolution decoder, our model can generate color more naturally while still maintaining colorfulness, indicating fewer miscoloring problems.

The impact of the s and the t_s in our self-attention guidance. The SAG scale is the s in Eq. (11). As shown in Fig. 17, as the scale s increases, the colors in larger adjacent regions tend to become more similar, which aligns with our expectations. We opted for a scale value that effectively eliminates color bleeding without excessively blending the colors, i.e. $s = 0.05$.

As mentioned in Sec. 3.2.3, we only change the \hat{e}_t between time step $t \in [T, t_s]$ during inference. Because the SAG process will increase the inference time and based on our experiments if $t_s \in [0, 600]$, the results won't have any visually visible difference when $s = 0.05$, thus, we choose $t_s = 600$ to minimize the potential increase in inference time. However, for these two parameters, especially s , different input images may have slightly different perfor-

mances, so we provide the options in our interface.

9. More Comparisons

As shown in Figs. 22, 23, 24, 25, 26, 27, 28, and 29, for unconditional colorization, we provided complete visual comparisons between our method and all the other methods mentioned in Tab. 2 in our main paper.

10. More Results

As shown in Fig. 18, we provide more visual results of our diverse unconditional image colorization on old photos and black and white films.

In Fig. 19, we provide some visual samples of our prompt-based image colorization.

Here we also provide more visual results to showcase the high controllability of our stroke-based colorization, as shown in Fig. 21. Notably, **our stroke-based colorization can modify any color details precisely** if the strokes are small enough, so that, even if there is any failure case that has a small color overflow or incorrect color, users can use our stroke-based method to fix it easily.

11. About Reproducibility

To ensure the reproducibility of our results, all our metrics in the document are calculated using results generated under $seed = 859311133$.

12. Limitations

For region coloring, our method may fail to generate very colorful regions if the original input image is grayscale and the region is relatively small. This is because we treat the other gray regions as the hints, so that the coloring for the specific region may be influenced by the gray hints. The result of the exemplar-based colorization may not be very similar to the exemplar if the exemplar's color is very complex. Although our method has shown promising and robust performance on image colorization, which is rarely achieved by existing methods. In some cases, our results may still have a color bleeding problem on very small objects or when the strokes are over the boundary. Fortunately, these issues can be solved by drawing a stroke on the bleeding area, as shown in our demo video.



Figure 18. Showcase of our diverse image colorization on old photos and black and white films.



Figure 19. Visual samples of our prompt-based colorization. Our model can colorize images based on text and can even incorporate words that describe the weather.

UniColor

CtrlColor (Ours)



"a single giraffe looks over the green brush"

UniColor

CtrlColor (Ours)



"a red stop sign with the word hammer time written on it"



"a blue and white train is moving on the rails"



"bedroom scene with a bookcase blue comforter"



"the tennis player wearing a purple outfit is about to hit the tennis ball"



"a yellow sign sitting in the middle of a road"



"a man holding a yellow surfboard walking into the ocean"

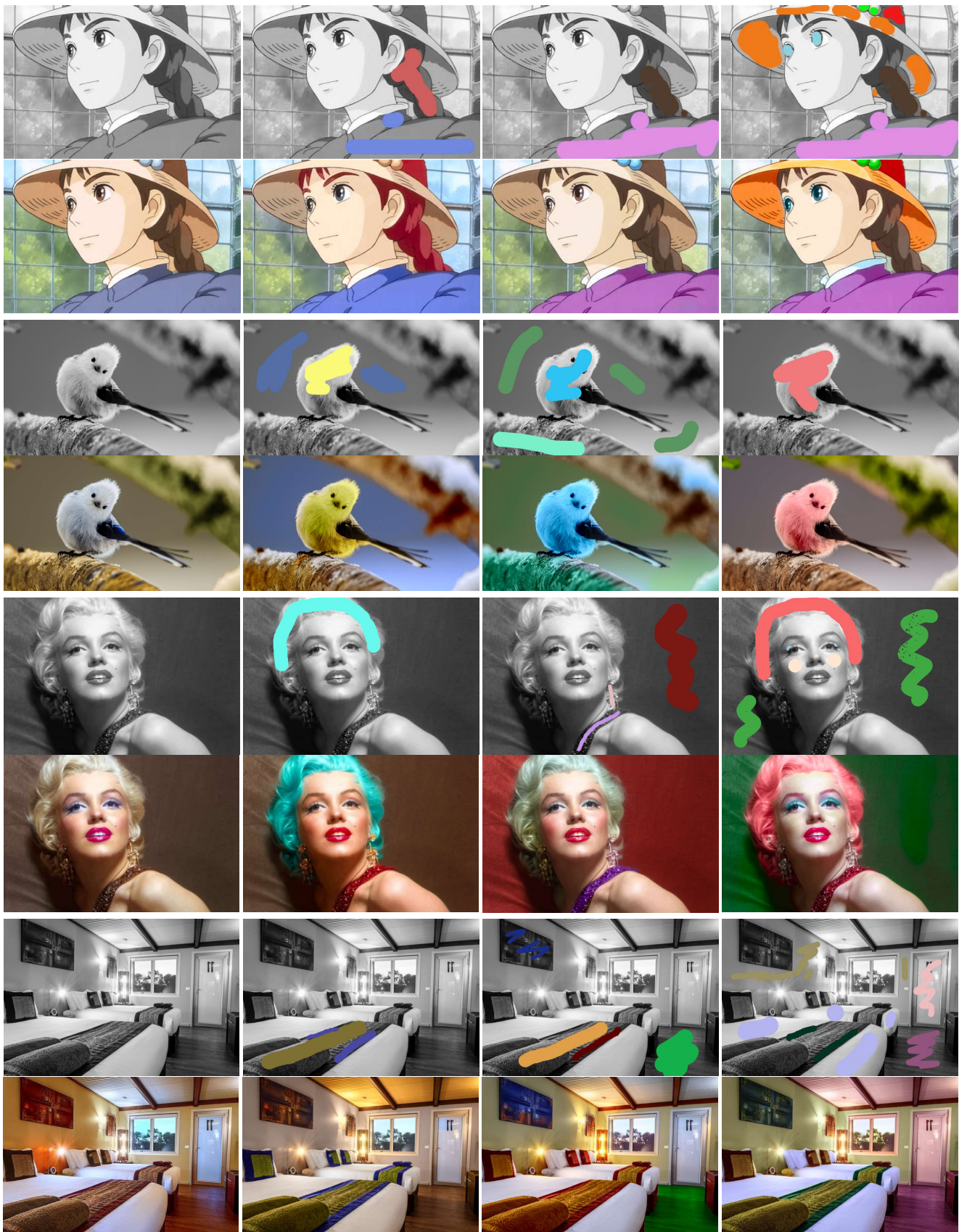


"a big purple bus parked in a parking spot"



"a city has colorful buildings and signs among cars"

Figure 20. More visual comparisons between UniColor [20] (left) and our CtrlColor (right). Our approach can generate vivid images that closely align with the given prompts.



Unconditional

Stroke-based Colorization

Figure 21. Visual samples of our stroke-based colorization. Our approach can generate vivid images that closely align with the given strokes.



Figure 22. Comparison with previous colorization methods on COCO validation set. Our CtrlColor produces images with the most color variation, separating the foreground person and the background shop windows.

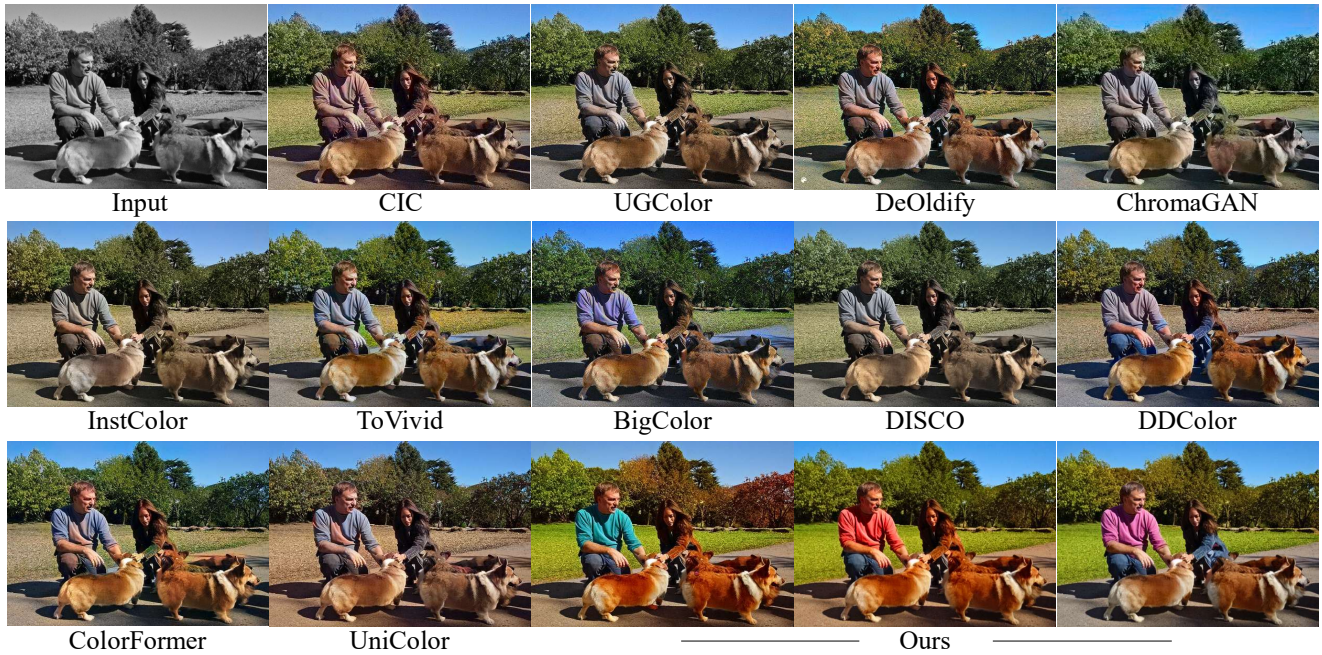


Figure 23. Comparison with previous colorization methods on ImageNet validation set. Our CtrlColor is able to generate diverse and vivid colors, specially notable between the clothes wore by the two persons.



Figure 24. Comparison with previous colorization methods on COCO validation set. Our CtrlColor differentiates color of tongue and lips from face, making the images more vivid and realistic.



Figure 25. Comparison with previous colorization methods on ImageNet validation set. Our CtrlColor produces more distinct colors and enhances the differentiation in details without color overflow.

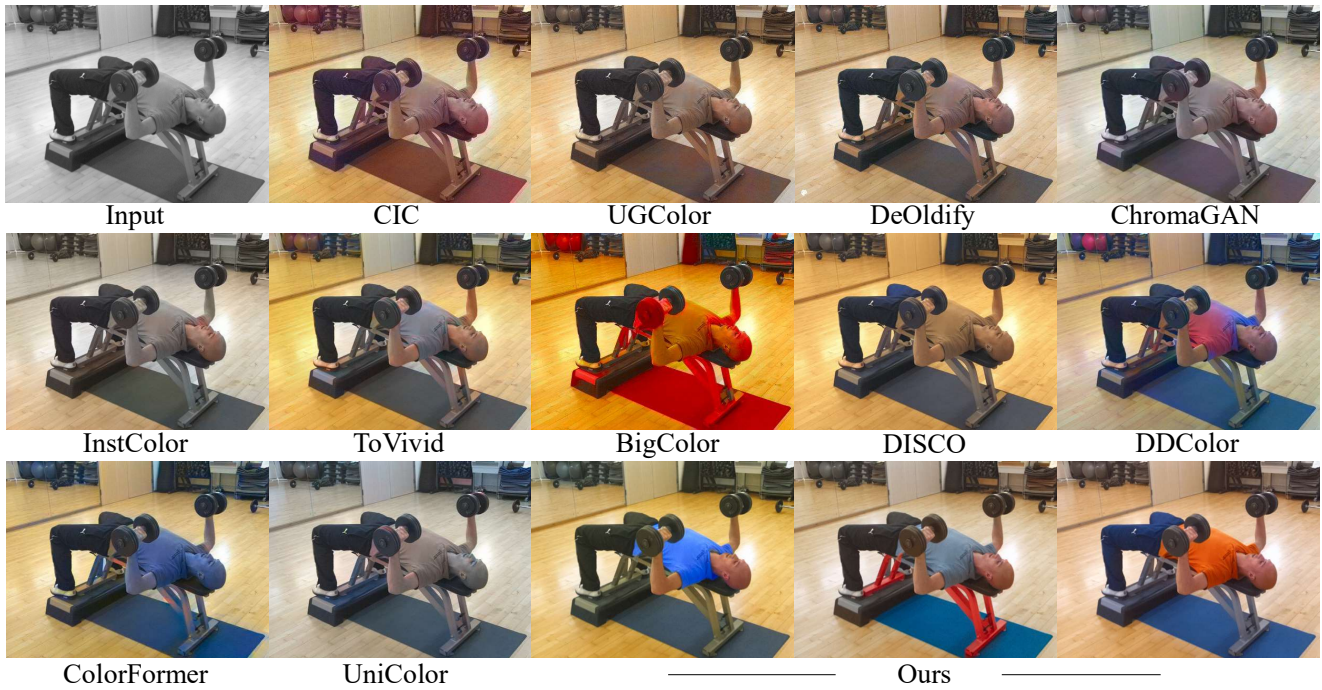


Figure 26. Comparison with previous colorization methods on ImageNet validation set. Our CtrlColor generates images with distinct color boundary between skin and clothes as well as equipment and exercise mat, with no color overflow.

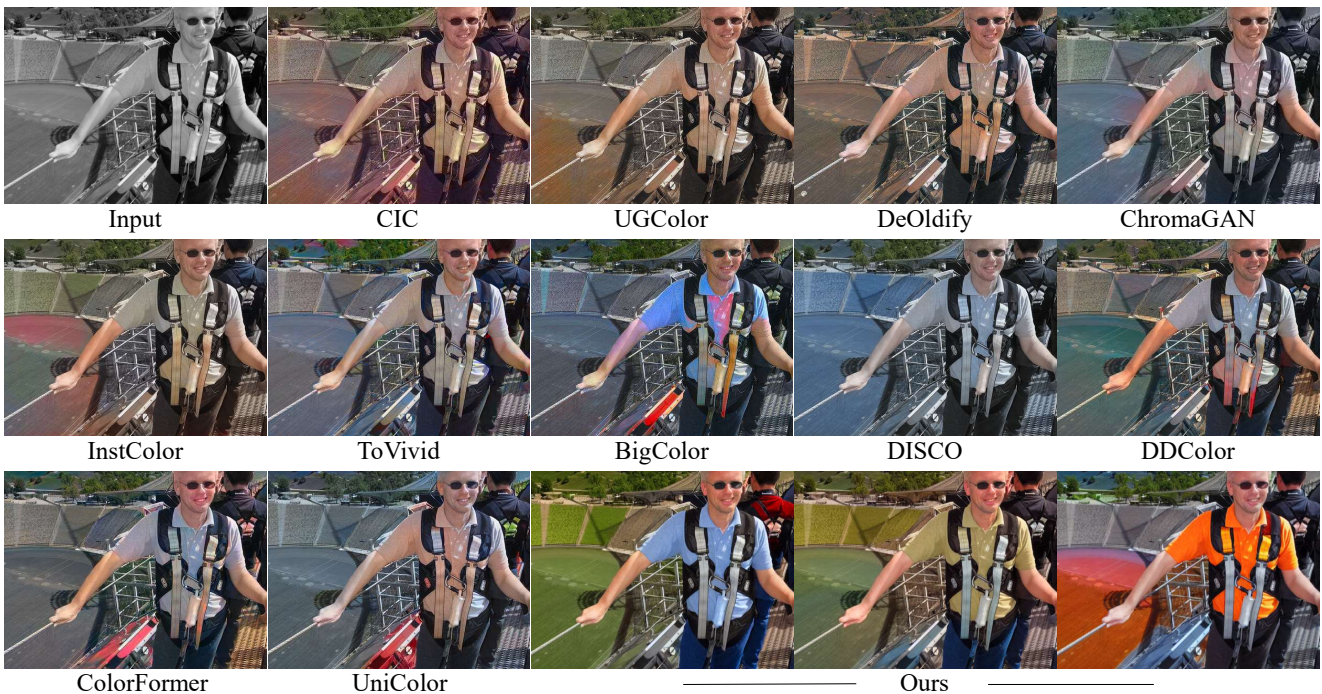


Figure 27. Comparison with previous colorization methods on ImageNet validation set. Our CtrlColor maintains color consistency in the image with complex information, clearly separating colors among the person's arm, T-shirt and bag, while all other methods suffer some degrees of color overflow.

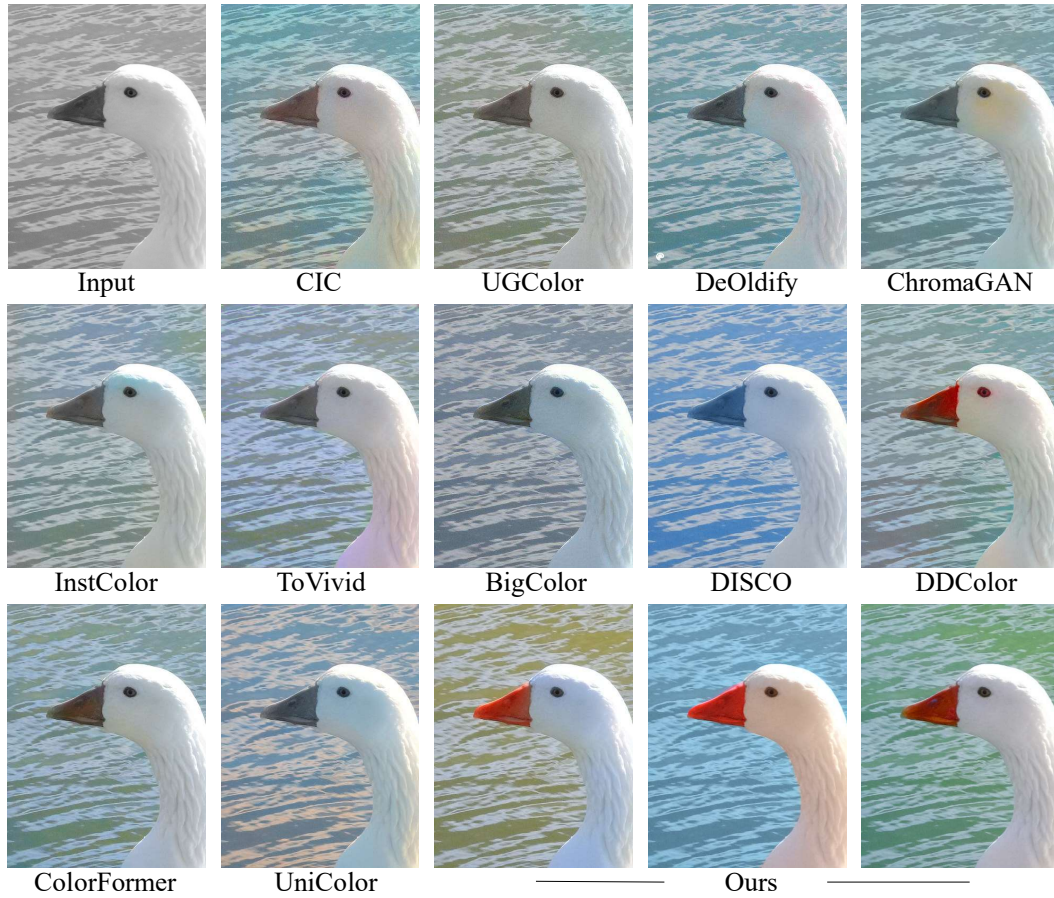


Figure 28. Comparison with previous colorization methods on ImageNet validation set. Our CtrlColor successfully colorizes the beak to red while maintaining a realistic color for the eye.

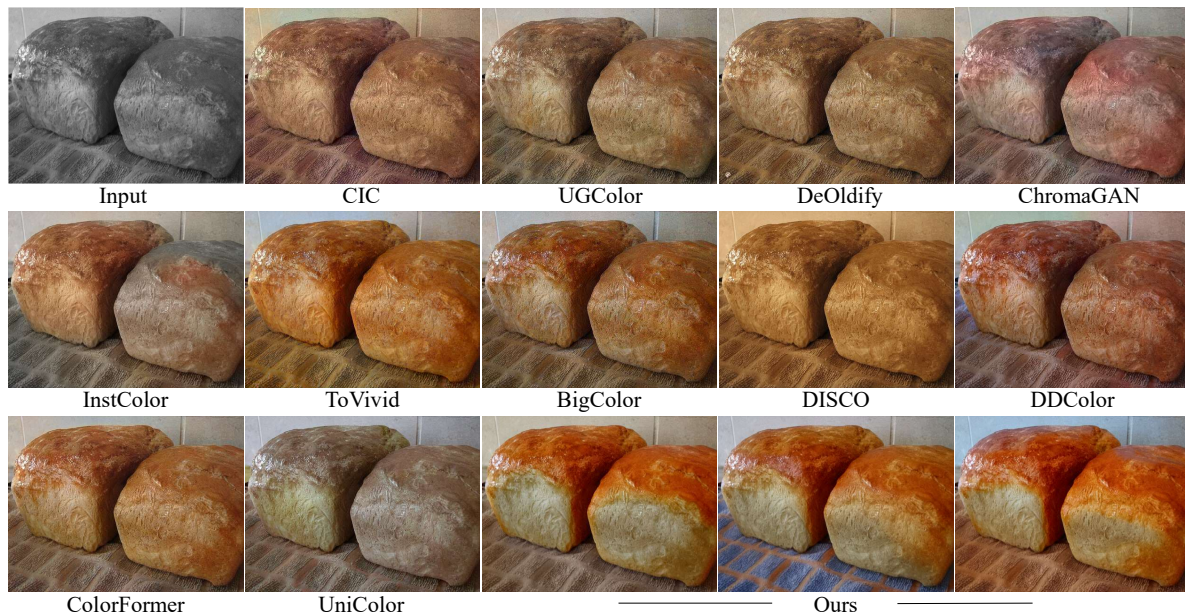


Figure 29. Comparison with previous colorization methods on ImageNet validation set. Our CtrlColor generates more vivid and realistic colors on the bread, making them look tastier. Our method also maintains clear color boundary between the bread and the food mat.